Coherent population transfer in multilevel systems with magnetic sublevels. III. Experimental results

J. Martin,* B. W. Shore,† and K. Bergmann
Fachbereich Physik der Universität Kaiserslautern, 67653 Kaiserslautern, Germany
(Received 15 February 1996)

The technique of stimulated Raman adiabatic passage (STIRAP) has become an established procedure for producing complete population inversion in atoms or molecules via application of Stokes and pump pulses in a counterintuitive sequence. Previously we reported on numerical and analytical investigations showing some of the additional and important phenomena that arise when some of the levels involved have nonzero angular momentum, the field polarization directions have no simplifying symmetries, and Zeeman splitting lifts the magnetic sublevel degeneracy. Here we verify our theoretical findings using the metastable neon system: $^3P_0 \Leftrightarrow {}^3P_1 \Leftrightarrow {}^3P_2$ with the corresponding angular momentum sequence $J=0 \Leftrightarrow J=1 \Leftrightarrow J=2$. In particular, we demonstrate that it is possible to transfer all population from the single initial state to any single selectable final magnetic sublevel M. Selectivity can be achieved either by choosing special laser polarization angles or, for fixed polarizations, by tuning the two lasers into two-photon resonance between the initial and desired final state. The complete control of magnetic sublevel population enabled by this procedure extends the customary experimental methods for producing oriented or aligned beams of atoms. In addition, we demonstrate very clearly the previous prediction that population transfer may fail for certain sets of parameters (detunings, Rabi frequencies, and polarization angles). [S1050-2947(96)03608-6]

PACS number(s): 42.50.Hz, 42.65.Tg, 42.65.Dr, 42.50.Fx

I. INTRODUCTION

A. Scope of this work

In the ongoing search for experimental techniques that will efficiently and selectively move population between stationary quantum states of atoms or molecules, schemes that use coherence of laser pulses have drawn increasing attention. The particular technique of stimulated Raman adiabatic passage (STIRAP) is becoming more and more popular amongst experimentalists. Proposed a decade ago as a theoretical curiosity [1], the remarkable properties of STIRAP were first demonstrated experimentally, and analyzed, by Gaubatz *et al.* [2–4]. Many other examples have been reported since then [5–12]. For a review of the related literature, already quite extensive, see [13]. Further theoretical discussion can be found in [14–18].

In simplest implementation the STIRAP procedure uses two pulses, applied to a three-state Raman system to move all of the population between an initially populated ground state (1) and a final state (3) that is targeted by the requirement of two-photon resonance. The final-state energy may be lower or higher than the intermediate-state energy. Here we deal with the former situation, the Λ configuration. The notable feature of STIRAP, as contrasted with other possible population transfer scenarios, is that the two pulses occur in counterintuitive order (i.e., the pump pulse, which couples the initial state to an intermediate one, arrives somewhat later than the Stokes pulse, which provides the connection to the final state). In the ideal STIRAP procedure, population is never placed in the intermediate state (2) of the three-state sequence, a state that would introduce population loss by spontaneous emission.

For many purposes related to STIRAP-type excitation it proves adequate to idealize the atomic or molecular system as comprising only three quantum states. However, any application to real atoms or molecules requires consideration of more complicated multistate systems, in which vibrational and rotational structure as well as hyperfine structure all introduce complications. The initial and final states may be embedded in a manifold of closely spaced states. The intermediaries may also be closely spaced or degenerate. Recent work has already clarified some aspects of multistate generalizations of STIRAP (for example, [17,19,20]) and have proposed interesting applications to quantum optics (for exampl, [9–12,15]). As in any coherent process, the possibility of multiple paths presents opportunity for constructive and destructive interference, and so it is to be expected that the excitation dynamics of multistate systems will exhibit phenomena not present with simpler systems.

The present paper presents experimental confirmation of recent theoretical work ([21,22], to be referred to as I and II) aimed at elucidating some of the physics of complete population transfer in degenerate (or nearly degenerate) systems. More specifically, we describe experiments in which atoms are prepared with arbitrary orientation of internal angular momentum, and we study the efficiency of the preparation process as we change such parameters as laser detunings, Rabi frequencies, and polarization angles.

A comment on terminology is useful. The literature of atomic and molecular physics disagree on names for the discrete structures between which radiative transitions occur. Here we tend to follow the tradition of atomic spectroscopy, rather than that of quantum chemistry. We refer to a ''state'' (or a magnetic sublevel or M state) meaning a nondegenerate

*Present address: Dept. of Chemistry, Stanford University, Stanford, CA 94305-5080.
†Permanent address: Lawrence Livermore National Laboratory, Livermore, CA 94550.

quantum state, for which further individualization is not possible. We use the term ''level'' when degeneracy is possible, meaning that a level may comprise several sublevels (or states). When there is no degeneracy, as is the case for the original three-state STIRAP, then there is no difference between a state and a level.

B. Review of basic theory

The simplest descriptions of pulsed multistate excitation rely on the time dependent Schrödinger equation. When used with the conventional rotating-wave approximation (RWA) the equation has the form ([23], Sec. 14.2):

$$\frac{d}{dt}\mathbf{C}(t) = -i\mathsf{W}(t)\mathbf{C}(t), \tag{1.1}$$

where $\hbar\mathsf{W}(t)$ is the (Hermitian) RWA Hamiltonian matrix of time t. The population $P_n(t)$ in state $n \in \{1 \ldots N\}$ at time t is given by the squared absolute value of the element $C_n(t)$ of the state vector $\mathbf{C}(t)$.

When pulse durations become comparable, or longer than, lifetimes for spontaneous emission, then the Schrödinger equation may fail to provide an adequate description of the system evolution. The effects of spontaneous emission are included by introducing an appropriate density matrix $\rho(t)$ and the concomitant Liouville equation (cf. [23], Sec. 6.3) Although we have used this approach in our extensive numerical modeling, we shall here use the simpler Schrödinger equation to interpret results.

As discussed in our previous papers (I and II) the instantaneous eigenvalues of $\hbar\mathsf{W}(t)$ are the adiabatic energies of the system, and the eigenvectors of $\hbar\mathsf{W}(t)$ are the adiabatic states at time t. Insight into the behavior of the system can be obtained by viewing plots of the time varying adiabatic energies, paying particular attention to near crossings or avoided crossings of the curves.

The increasing size of the Hamiltonian matrix that accompanies the inclusion of many states complicates the theoretical and numerical treatment. Simple algebraic methods presented in Ref. [22] (and relying on properties of the determinant of the Hamiltonian matrix) help to identify situations in which complete population transfer may take place. The essential idea is to identify a *stationary adiabatic state*, defined as a solution $\mathbf{C}(t)$ to the equation

$$\mathsf{W}(t)\mathbf{C}(t) = 0. \tag{1.2}$$

If we find such a zero-eigenvalue dressed state available throughout the interaction with the laser pulses, we call it a *trapped state*. If one or more elements $C_n(t)$ of this state stay zero throughout, they will not receive any population. We call the corresponding bare atom state a *dark state*. If all intermediate states of a STIRAP sequence are dark states then $\mathbf{C}(t)$ becomes an *ideal state to transfer population*. Such ideal cases have been theoretically analyzed for four- and five-state sequences [20,24,25], and Ref. [17] considered some specific situations for cases where the pump and Stokes lasers couple multiple intermediate or final states.

C. Results from papers I and II

The present work verifies experimentally, using a metastable neon atomic beam, the theoretical predictions of previous papers I and II. We have shown there, with computations based on the Liouville equation to allow the inclusion of spontaneous emission, that it should be possible to obtain complete control of the orientation of atoms in an atomic beam, by simply changing the frequency of one of the excitation lasers. Polarization directions of the lasers remains fixed, and selectivity is achieved by meeting the two-photon resonance condition. As in our previous papers I and II, we consider linearly polarized light, propagating perpendicular to the static external magnetic field. We take the angle between pump-laser polarization and this external reference axis to be β_P. The corresponding Stokes polarization is specified by angle β_S. The polarization of each laser beam is uniquely defined by a single angle, because both laser beams propagate colinearly; they are perpendicular to common axis of the magnetic field and the atomic beam axis, which we choose as the quantization axis. We have shown in papers I and II that, in the case of multiple couplings to intermediate and final states, ideal transfer situations occur only for special polarization choices. These lead mostly to simplifications of the scheme to isolated three- and four-state systems. In the general case of multiple couplings an inspection of the instantaneous eigenvalues of the RWA Hamiltonian makes it obvious that for a variety of parameter ranges the curves show crossings or avoided crossings. High population transfer rates can be achieved only if a set of restrictive conditions apply.

Any STIRAP-like population transfer scheme requires that when the pump pulse is absent, initially, there must be a single adiabatic dressed state that coincides with the initial atomic state. Furthermore, to prevent loss by spontaneous emission, the state vector should at all times have negligible component of any intermediate sublevel. Finally, there should be a unique adiabatic state that coincides with the desired final state at the completion of the two-pulse sequence. In our previous work we identified some additional key issues that must be considered when attempting multistate population transfer by STIRAP pulse sequences (and there are more than three states involved in the linkage).

Adiabaticity: In the case of an ideal transfer state the system should remain in a single adiabatic state, the stationary zero-eigenvalue adiabatic state. However, when multiple couplings occur there are cases where transfer fails *even though* the evolution is completely adiabatic, and there exist other cases where high transfer efficiencies are observed *because* of fast nonadiabatic curve crossings.

Connectivity: When the Stokes pulse is absent, toward the conclusion of the counterintuitive pulse sequence, the adiabatic state of interest should coincide with the desired final state. This must connect, either via traditional adiabatic evolution or by diabatic evolution near curve crossings, with the initial adiabatic state.

In cases with nonideal transfer states predictions of success or failure of population transfer require detailed examination of adiabatic energy curves, with attention to the issues of adiabaticity and connectivity. As has been outlined in [21] one of the most interesting cases is the failure of connectivity between initial and final null-eigenvalue adiabatic states.

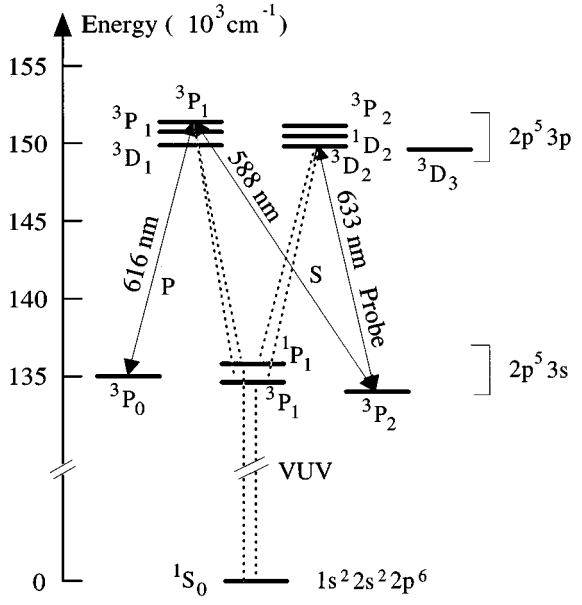

FIG. 1. Levels and transitions of the neon atom relevant for this experiment. The STIRAP fields couple the $^3P_1$ and $^3P_2$ levels (Stokes laser, S) and the $^3P_1$ and $^3P_0$ level (pump laser, P). The populations of the level $^3P_2$ is monitored by detecting the vuv radiation which follows as a cascade transition the excitation to the level $^3D_2$ with subsequent decay to one of the two levels $^{3,1}P_1$.

That is, when only the Stokes field is present there occurs a null-eigenvalue dressed state that is identical with the initial state, and when only the pump field is present (finally) there is a null-eigenvalue state coinciding with the target final state, but these two dressed states are not connected adiabatically. In a well defined range of laser detunings and magnetic-field splittings (and sometimes Rabi frequencies) transfer is impaired or not even possible. Such an inhibition may occur despite the fact that all conventional STIRAP conditions apply and the evolution remains completely adiabatic.

II. EXPERIMENT

A. Neon as a model system

We consider a model system involving three levels, whose angular momenta J_1, J_2, and J_3 are not all zero. The magnetic moments associated with the angular momenta provide the means to control the energy splitting of the magnetic sublevels in a constant external magnetic field. Ne* atoms, readily and efficiently prepared in their metastable triplet levels in a discharge source, offers an excellent choice of system. Figure 1 shows the neon ground level and the sets of states resulting from two excited $2p^5\,3s$ and $2p^5\,3p$ electron configurations. The levels $^3P_0$ and $^3P_2$ of the $2p^5\,3s$ configuration are the metastable levels of interest here. They are coupled to the short lived $^3P_1$ intermediate level by pump and Stokes lasers in the visible range ($\lambda \approx 600$ nm). The transition dipole moments are relatively large, so that strong coupling of these levels can be achieved with laser powers of only a few mW. Because of magnetic sublevel degeneracy,

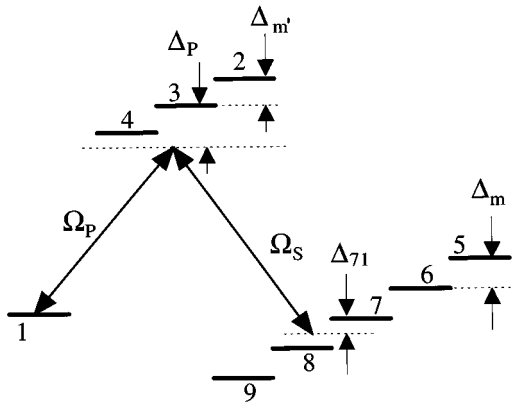

FIG. 2. Nine-state system. The coupling between the group of states is determined by the pump-laser Rabi frequency (Ω_P) and by the Stokes-laser Rabi frequency (Ω_S). The Zeeman splittings in the intermediate and final level are $\Delta_{M'}$ and Δ_M, respectively. The detuning of state k from the two photon resonance with state 1 is Δ_{k1}.

the system consists of an initial state, three intermediate states and five final states (see Fig. 1). Depending on the choice of polarizations, the coupling establishes an N-state scheme with N between 3 and 9, illustrated in Fig. 2.

The magnetic moment of the $^3P_1$ and the $^3P_2$ levels is nonzero and so an external magnetic field can be used to control the Zeeman splitting by $\hbar\Delta_m = g_J \mu_B B_0$ in three or five magnetic sublevels, respectively.

All the relevant quantities such as wavelengths, lifetimes, and g factors are given in Table I. The Clebsch-Gordan co-

TABLE I. Lifetimes τ (in units of 10^{-9} s), g-factors g_J, wavelengths (in nm) and Einstein coefficients A_{ij} relevant for the present experiment. The rows are formed by the first electronically excited 3s configurations and the columns by the 3p configurations. The matrix entries represent the data for transitions between these levels. The upper value gives the transition wavelength, the lower value the Einstein coefficient in units of 10^7 s.

$2p^5 3s \rightarrow$	$1s_5\,^3P_2$	$1s_3\,^3P_0$
	$\tau > 0.8$s[a]	$\tau > 0.8$s[a]
$\downarrow 2p^5 3p$	$g_J = 1.501 \pm 0.004$[b]	
$2p_2\,^3P_1$	588.190	616.359
$\tau = 18.28 \pm 0.07$[c]	1.10 ± 0.05[d]	1.51 ± 0.07[d]
$g_J = 1.3397(6)$[e]		
$2p_8\,^3D_2$	633.443	
$\tau = 19.56 \pm 0.04$[c]	1.79 ± 0.07[d]	
$g_J = 1.1364(8)$[e]		

[a]R.S. van Dyck, C.E. Johnson, and H.A. Stuart, Phys. Rev. A **5**, 991 (1972).

[b]E. Pinnington, J. Opt. Soc. Am. **57**, 271 (1967), essentially a confirmation of the previous results of A. Back, Ann. Phys. (Leipzig) **76**(4), 317 (1925).

[c]S. Kandela and H. Schmoranzer, Phys. Lett. A **86**, 101 (1981), and references therein.

[d]P. Hartmetz and H. Schmoranzer, Z. Phys. A **317**, 1 (1984).

[e]E. Giacobino, J. Phys. (Paris) **38**, 1377 (1977), the number in parentheses gives the uncertainty in the least significant digit.

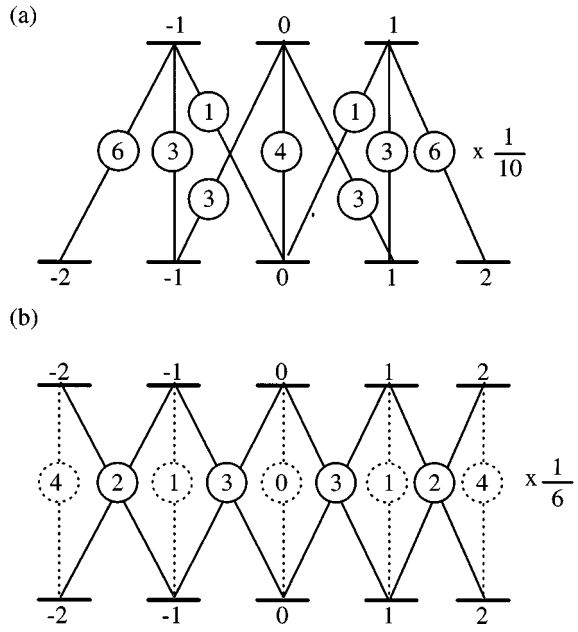

FIG. 3. The square of the Clebsch-Gordan coefficients for (a) $J=1\Leftrightarrow J=2$ and (b) $J=2\Leftrightarrow J=2$ electric-dipole transitions.

efficients for $J=1\Leftrightarrow J=2$ and $J=2\Leftrightarrow J=2$ transitions are given in Fig. 3. The latter transition is used for detecting the population transfer.

The convenience of production and excitation, together with the flexibility in choosing the coupling scheme and controlling state splitting, as well as the absence of hyperfine splitting, make metastable neon atoms an ideal system for the study of coherent population transfer in multistate systems. Furthermore, the population of the metastable levels can be conveniently monitored by the efficient and nearly background-free detection, with a channeltron, of the vacuum ultraviolet (vuv) fluoresence radiation which follows laser excitation to the $^3P_1$ level [26,27].

B. The Ne* beam and the lasers

A schematic representation of the apparatus is shown in Fig. 4. The mean velocity of the particles in the beam is 800 m/s and the width of the velocity distribution is 200 m/s. The atomic beam propagates through a three-stage differentially pumped vacuum system. The first chamber contains a cold cathode discharge source from which the beam expands through a 0.8 mm diameter nozzle and a skimmer into the second chamber. There a beam from a Coherent 599 linear dye laser system intersects the atomic beam at a right angle. The wavelength of this preparation laser is tuned to $\lambda=588.190$ nm in order to deplete the population of the metastable $^3P_2$ level by optical pumping via the $^3P_1$ level. Elimination of the population of all magnetic sublevels is assured when the laser power is of the order of 50 mW and the beam diameter is sufficiently large (about 10 mm), to allow enough time for magnetic sublevel mixing due to Larmor precession induced by the stray magnetic field. Downstream of this preparation region only atoms in the metastable level $^3P_0$ remain in the beam and the transfer of the population of this level to the various M states of the level $^3P_2$ can be studied.

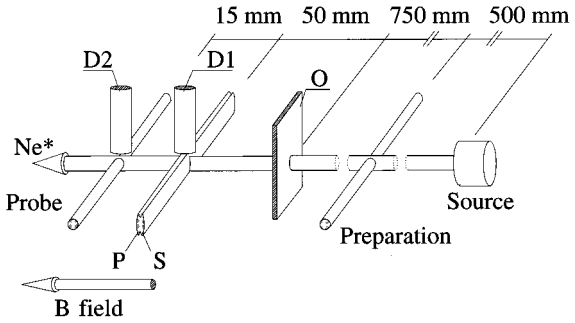

FIG. 4. Schematics of the experimental setup. A beam of metastable Ne* atoms from a discharge source is collimated by a 1 mm diam orifice (O) to about 1: 10^3. The preparation laser depletes the population in the level $^3P_2$ by optical pumping. Cylindrical lenses are used to focus the pump laser (P) and the Stokes laser (S). Their overlap is controlled with the aid of beam splitter cubes. Fluorescence from the region where the STIRAP transfer occurs is monitored by detector D1. The population in the level $^3P_2$ is monitored by the probe laser in conjunction with detector D2. Both detectors are channeltrons which record vuv photons (see Fig.1).

Further downstream the neon atoms enter the vacuum chamber containing the STIRAP interaction and detection region. This chamber is differentially pumped and separated from the previous stage by a long (300 mm) and thin (16 mm diam) tube. 50 mm upstream of the interaction region with the lasers that induce the STIRAP transfer, the beam passes through a 1 mm diam orifice. The distance between this orifice and the nozzle of the beam source is 1250 mm. Thus the atomic beam is collimated to about $1:10^3$. The pump laser and the Stokes laser for the STIRAP process, each one with a power of the order of 50 mW, are guided by single mode optical fibers from Coherent 699 ring dye laser systems, tuned to 616.359 nm and 588.190 nm, respectively. Diaphragms and cylindrical lenses shape the laser beams as needed. The linear polarizations and the intensities of the lasers are controlled with the aid of various polarizers and $\lambda/2$ plates.

The natural linewidth of the fluorescence from the $^3P_1$ level (the intermediate level) is about 9 MHz and is thus large compared to the residual Doppler width of about 1 MHz and the 2 MHz bandwidth of the lasers. Therefore if line broadening is observed in the experiments, it is determined by the degree of saturation broadening.

The atoms cross the laser fields at right angle. The temporal profile of the laser fields seen by the atoms is determined by the spatial profile of the laser beams. This spatial profile of the beams and their overlap is controlled and adjusted using a charge-coupled device (CCD) camera.

The channeltron detector D1 (see Fig. 4) monitors the vuv radiation at 74 nm emitted from the intermediate level in the STIRAP zone in the second step of a radiation cascade (see Fig. 1). The signal of D1 is used to control the tuning of the lasers with respect to the resonance of their respective transition. It is also used to observe the dark resonance associated with efficient population transfer.

The channeltron detector D2 monitors the population transferred to the $^3P_2$ level, again through the vuv radiation induced by a fourth laser (the probe laser). Radiation from this laser (Coherent 699 ring dye laser) pumps the

$^3P_2 \Leftrightarrow {}^3D_2$ transition at 633.443 nm. This latter level decays also to the $^1P_1$ and $^3P_1$ electronic levels which subsequently decay to the $^1S_0$ ground state. The pressure in the chamber containing the detectors D1 and D2 did not exceed 10^{-7} mbar. At a higher pressure scattering of metastable atoms off particles in the residual gas may deflect them to the surface of the channeltron causing a large background signal.

A homogenous magnetic field parallel to the atomic beam axis is established by two Helmholtz coils in the regions covering the STIRAP transfer zone and the detection area. The direction of this magnetic field, which is used as a guiding field or to control the Zeeman splitting, defines the quantization axis used throughout this work. It is aligned parallel to the atomic beam axis.

C. Calibration procedure

The main concern of this work is to characterize important properties of the population transfer process and to identify situations where efficient transfer may fail. Another issue is the determination of the absolute transfer efficiency. For the latter we needed to devise a calibration procedure.

Calibration is required when we are interested in the transfer to a specific single M state of the final level or when we are (only) interested in the transfer to the $^3P_2$ final level irrespective of the distribution of the population over the M states. In both cases calibration relies on the known branching ratios of the fluorescence from the intermediate $^3P_1$ levels to the final M states of the $^3P_2$ level. Assuming full depletion of the initial $^3P_0$ level by optical pumping, when only the pump laser is present, we can predict which fraction of that population has reached the final $^3P_2$ level [3].

Individual M-state detection is possible when the Zeeman splitting is large enough compared to the saturation broadened linewidth. The ability to detect single M states relies on the difference of the g factors in the upper and lower level and on a high collimation of the atomic beam. To avoid saturation broadening the probe-laser power must be very low, in the range of only a few μW or even less.

The STIRAP and detection region are both covered by a uniform magnetic field. When the B field is nonzero but too small to allow resolution of single magnetic substates, we follow another strategy. We use a probe laser with sufficient power (typically more than 25 mW) to induce strong saturation broadening. When the broadening exceeds the frequency difference between the $M=2 \Leftrightarrow M'=1$ and the $M=-2 \Leftrightarrow M'=-1$ transitions and the polarization angles are chosen to ensure strong coupling of all participating transitions, uniform excitation probability is assured.

When the Zeeman splitting is large, but not large enough to avoid partial overlap of the laser line and some $M \Leftrightarrow M'$ transitions, it is difficult to determine the transfer efficiency. We avoided this situation because it permits neither complete M-state resolution nor uniform, M-independent excitation probability. Also, evaluation of the population distribution over the M states established by spontaneous emission during the detection process becomes complicated.

The transfer efficiency is determined by comparing the maximum intensity of the laser-induced fluorescence from the final level with only the pump laser on (S_P) and under STIRAP conditions with both pump and Stokes laser on ($S_{P\&S}$). The signal S_P is determined by the spontaneous emission from the intermediate to the final level. The signal ($S_{P\&S}$) is proportional to the population of the final state or level due to coherent population transfer. The ratio of these intensities

$$T=\gamma\frac{S_{P\&S}}{S_P} \tag{2.1}$$

yield the transfer efficiency T, where γ is the branching ratio of the radiation from the intermediate level into the target level or the particular M state under consideration.

The phenomena observed when detecting the fluorescence following excitation by a laser field in a uniform magnetic field with linearly polarized light are discussed in detail in Ref. [28]. Here we apply those results to our experimental conditions.

1. Single M-state detection

First we discuss the case when the population of an individual M state is probed. We need to find a compromise between sufficiently high laser power to assure a uniform detection efficiency independent of M and a sufficiently low laser power to avoid detrimental power broadening.

An illustration is given in Fig. 5 using the thermal population of the level $^3P_2$ as an example. A magnetic field of 60 G was applied. The laser polarization of the probe laser was perpendicular to the magnetic-field direction for the data shown in panels (a) and (b) but parallel for panels (c) and (d). The transitions between magnetic quantum numbers of the lower (M) and upper (M') state are given as (MM') in the panels (a) and (c). The left and right groups of lines in panels (a) and (b) are related to $\Delta M=-1$ and $\Delta M=+1$, respectively. The Zeeman splitting is clearly visible in all four cases. However, even at a laser power as low as 9 μW the saturation broadening is substantial. The laser power needs to be reduced to the order of 500 nW to resolve fully the transitions between individual M states. The selection rule $\Delta M=0$ applies for the spectra shown in panels (c) and (d) with the transition (0 0) missing.

When the probe-laser power is reduced to 500 nW the transitions are not saturated and the ratios of peak intensities approach the values expected from the ratios of Clebsch-Gordan coefficients related to the excitation path (see Fig. 3 for these values). Small deviations from these theoretical ratios are attributable to the angular distribution of the vuv radiation (see below).

At higher laser power the excitation probability approaches unity, independent of the transition probabilities, but individual (MM') transitions are still identified. This indicates, that we have reached the range of the required compromise mentioned above. We will lose the M resolution when the laser intensity is further increased. In the case of ideal detection the observed peaks should all have equal heights. The small differences in the peak height, even under conditions of substantial power broadening in panel (a), are related to the angular distribution of the vuv radiation. The detector's axis of symmetry is perpendicular to the direction of the magnetic field and thus perpendicular to the quantization axis. The fraction of photons emitted into the solid angle

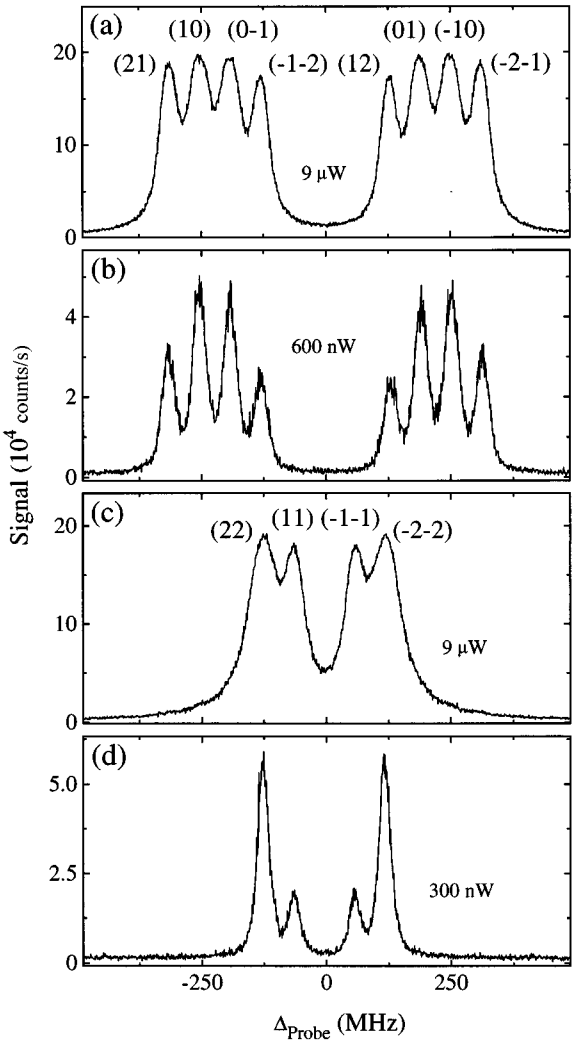

FIG. 5. Demonstration of the M-state selectivity of the detection with the probe-laser polarization perpendicular [(a) and (b)] and parallel [(c) and (d)] to the magnetic field. The Zeeman components are clearly resolved for a laser power <600 nW. At this magnetic field ($B=60$ G) saturation broadening prevents detection of an individual M state for probe-laser power exceeding 10 μW.

seen by the detector depends on ΔM. The detection efficiency of photons related to a $\Delta M=0$ transition is slightly higher as compared to $\Delta M=\pm 1$. The innermost peaks of panel (a), labeled $(-1\ -2)$ and $(1\ 2)$ result from the excitation to the $M'=\pm 2$ state of the $^3D_2$ level which decays only to the $M=\pm 1$ states of the $^{3,1}P_1(2p^5\ 3s)$ levels. Subsequent decay to the ground state occurs via $\Delta M=\pm 1$ while other decay paths also include $\Delta M=0$ transitions. This explains why detection of radiation involving decay via the $M'=\pm 2$ states in the $^3D_2$ level is slightly discriminated [panel (a)].

During the excitation process part of the population falls spontaneously back into neighboring magnetic sublevels and does not contribute to the fluorescence seen by the vuv detector. If the polarization of the excitation laser is perpendicular to the quantization axis [panels (a) and (b)], the loss due to population falling back into unconnected states is nearly the same for all possible ΔM transitions (see the Clebsch-Gordon coefficients in Fig. 3). In the case of parallel

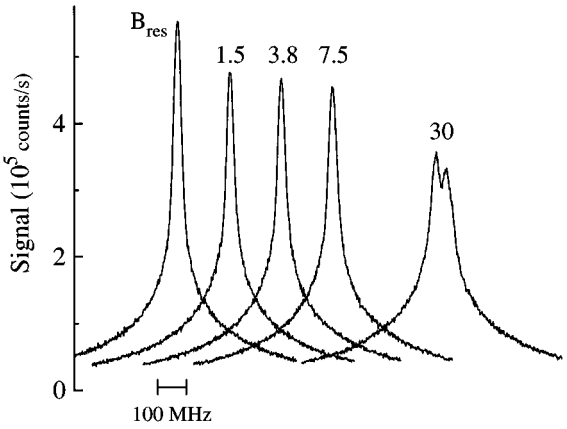

FIG. 6. Laser induced vuv fluorescence from the level $^3P_2$, populated in the discharge source, observed by detector D2 (see Fig. 3) for different magnetic fields and under conditions of strong saturation broadening. The polarization vector ϵ_{pr} of the probe laser is parallel to the magnetic field. For better visibility the spectra are horizontally displaced. Only the residual magnetic field (B_{res}) was present when the spectral line shown at the left was recorded. Because B_{res} and ϵ_{pr} are not parallel, Larmor precession mixes the M states such that the population of all M states is monitored. The other lines are labeled by the applied magnetic fields (B measured in G). In these cases, the direction of the probe-laser polarization and the B field coincide. Therefore the population of the state $M=0$ is not monitored and the maximum signal is reduced accordingly. Zeeman splitting of the lines is observed for $B=30$ G.

excitation [panels (c) and (d)] pumping of transitions $(\pm 1\ \pm 1)$ lead to more than twice as much loss into unconnected states of the $^3P_2$ level than pumping transitions $(\pm 2\ \pm 2)$. This enhancement overcompensates the reduction in the detection probability, discussed previously. The net result is slightly smaller peak heights of the $(1\ 1)$, $(-1\ -1)$ compared to the $(2\ 2)$ $(-2\ -2)$ transitions [panel (c)].

2. Integral detection

The population distribution over the M states established by spontaneous emission when only the pump laser is present is different from that established by STIRAP. Unlike when the detector fully resolves M states, this difference matters. Excitation-emission cycles redistribute the population among the M states while the atoms are exposed to the detection laser. However, this redistribution tends to reduce the small differences in the detection probability due to the angular distribution of the vuv emission. Also, if the polarization vector of the detection laser is parallel to the direction of the magnetic field, population accumulates in state $M=0$. When the magnetic field is sufficiently strong to dominate stray fields, the population of the $M=0$ state cannot be detected via the $^3P_2 \Leftrightarrow {}^3D_2$ transition with linear polarizations.

It is best to apply a magnetic field which leads to a Zeeman splitting small compared to the saturation broadened linewidth but which is sufficiently large (typically 5 G) to dominate residual stray fields.

Figure 6 illustrates what was discussed above, with the thermal population of the $^3P_2$ level as an example (see also

Ref. [28]). When no current is applied to the Helmholtz coils, only the residual stray magnetic field B_{res} is present. This field is not parallel to the direction of the linear polarization of the probe laser ϵ_{pr}. Larmor precession mixes the M states and all the population is detected. As soon as a sufficiently large external field ($B>1$ G) parallel to ϵ_{pr} is applied, the state $M=0$ can no longer be detected and the signal decreases by 20% as expected. For $B>30$ G the Zeeman splitting exceeds the power-broadened spectral linewidth. This field value marks the transition to a regime where individual M state detection becomes possible.

In summary, we have shown in this section how to quantify the transfer efficiency from the initial to the final level. We have furthermore shown that for small magnetic fields (<10 G) integral detection and for large magnetic fields (>60 G) individual M state resolution can be achieved with our detection scheme. The latter possibility will be used to demonstrate the M-state selectivity of the STIRAP transfer process, as discussed in the next section.

III. RESULTS AND DISCUSSION

It is a remarkable property of the STIRAP transfer process that individual M states can be selectively populated. As the numerical studies of paper I showed, the orientation of the electronic angular momentum can be changed from $M=-2$ to $M=+2$ simply by tuning the laser frequencies to the appropriate two-photon resonances, provided the angles of linear polarizations are chosen such that a sufficiently strong coupling is established between the initial level ($^3P_0$) and the final M state. It is therefore important to show experimentally that a high M selectivity can indeed be achieved. This is demonstrated in Fig. 7, where we compare the distribution of population over the M states of the final level $^3P_2$ established by spontaneous emission [panels (b) and (d)] and by STIRAP transfer [panels (a) and (c)].

In this case the pump-laser polarization was aligned parallel to the magnetic-field direction. Therefore only the $M'=0$ state of the $^3P_1$ level is radiatively coupled to the initial level $^3P_0$. From the former level the states $M=\pm1$ and $M=0$ in the final level $^3P_2$ are populated by spontaneous emission. This population distribution is monitored by the probe laser, the polarization of which is set either parallel to the magnetic-field direction [panels (a) and (b)] or perpendicular to it [panels (c) and (d)]. In the former case, see panel (b), the two groups of three lines correspond to $\Delta M=\pm1$. These lines show the population of $M=\pm1$ and $M=0$ which is established by spontaneous emission. When the probe laser polarization is parallel to the magnetic field [panel (d)] the state $M=0$ is not detected. If the population transfer occurs via STIRAP either two strong lines from $\Delta M=\pm1$ transitions out of $M=0$ are seen (these lines exceed the maximum signal arising from population by spontaneous emission by more than a factor of three) or none are seen [panel (c)]. In the latter case, the population of $M=0$ cannot be detected and only the spurious population of states $M=\pm1$ gives rise to a small signal.

Quantitative analysis of signals such as those presented in Fig. 7 shows that transfer efficiencies exceeding 98% have been achieved. In all cases shown below the maximum transfer efficiency exceeds 80%.

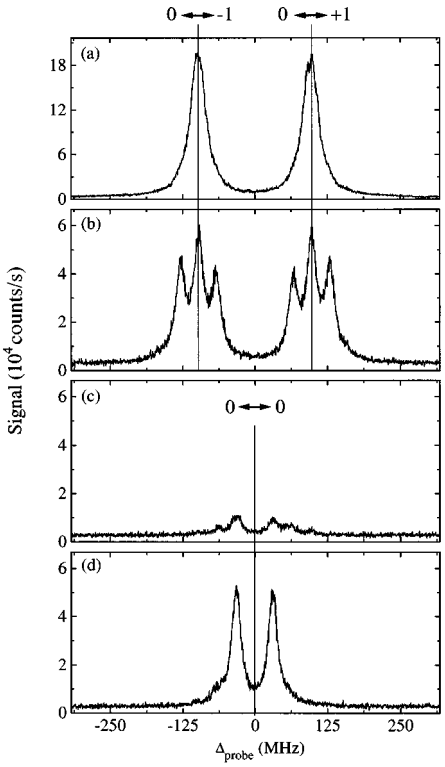

FIG. 7. Demonstration of the M-state selectivity of the transfer process. The magnetic-field strength is about $B=60$ G. The intensities of the pump laser, Stokes laser, and probe laser are $I_P=2.7$ mW, $I_S=22$ mW, and $I_{probe}=14$ μW, respectively. The probe-laser polarization is perpendicular to the magnetic field in panels (a) and (b), it is parallel in panels (c) and (d). The population in the final level $^3P_2$ is established by spontaneous emission [panels (b) and (d)] or by STIRAP [panels (a) and (c)].

A. The three-state case

Selective transfer of population to a specific M state of the final level is best achieved when the coupling scheme, determined by laser polarization, comprises only three states. When the linear polarization of the lasers is parallel to the magnetic field, only the $M=0$ states of the initial, intermediate, and final level are coupled. They form a three-state system, as desired for the implementation of STIRAP in its simplest form. We show some data for this situation, for comparison with results from more complex level schemes, presented thereafter.

Figure 8 displays in the upper part the laser-induced fluorescence signal from the final state, as seen by detector D2 as the pump-laser frequency is tuned. Efficient population transfer occurs when the two-photon resonance $\Delta_P=\Delta_S=0$ holds. The fluorescence from the intermediate level as seen by detector D1, shown in the lower part, appears as a dark resonance. This is a signature of the formation of the trapped state. As the pump laser is tuned, but without establishing a two-photon resonance between the initial and final state, we observe with detector D1 a substantially saturation broadened fluorescence emission line from the intermediate state. Detector D2 monitors the population of the final state established by that same spontaneous emission. In this case, the Stokes laser is detuned by about 200 MHz from the one-photon resonance. Coherent population transfer and the for-

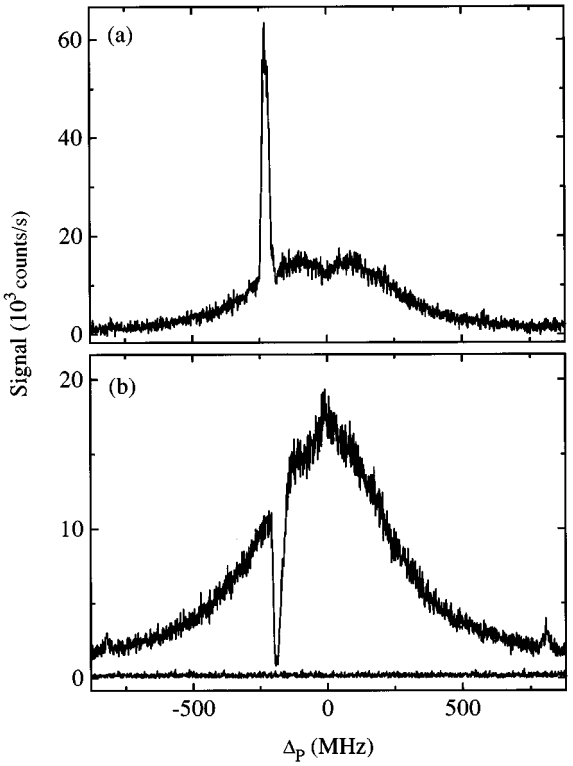

FIG. 8. Population transfer (a) and associated dark resonance (b) when both the pump-laser and Stokes-laser polarization is parallel to the magnetic field ($B=15$ G). The pump laser is tuned across the resonance as the Stokes-laser frequency is held at about 200 MHz of the one-photon resonance. The power of both lasers was 60 mW. The signals shown are recorded sequentially. A small drift of the Stokes-laser frequency is responsible for the fact that the maximum of the transfer and the minimum of the dark resonance do not coincide precisely.

mation of a dark resonance is thus observed 200 MHz off the maximum of the saturation broadened line. Evaluation of the transfer efficiency according to Eq. (2.1) yields, for this choice of polarizations, a transfer efficiency of 95 %.

Figure 9 shows the signal seen by the detector D2, which is proportional to the population in the final state $M=0$ of the $^3P_2$ level. The pump-laser frequency is tuned, as the Stokes-laser frequency is changed in increments. Tall peaks are seen for the two-photon resonance $\Delta_P=\Delta_S$. For increased one-photon detunings the transfer efficiency decreases slightly because the adiabaticity criterion is only marginally fulfilled. The decreasing width of the two-photon line also reflects this behavior. It is, however, noteworthy that substantial transfer is still possible when lasers are detuned by more than 200 MHz. The broad feature is proportional to the population in $M=0$ ($^3P_2$) established by spontaneous emission.

The small dips in the center of the broad structure of the laser-induced fluorescence out of the final level, seen in Figs. 9 and 8, are the result of depletion due to optical pumping by stray light. In fact, it has been noted before that even small amounts of spurious stray light may be detrimental to the efficiency of coherent population transfer. This is particularly true when the laser frequencies are tuned to the one-photon resonance. Depletion of the $^3P_0$ metastable level

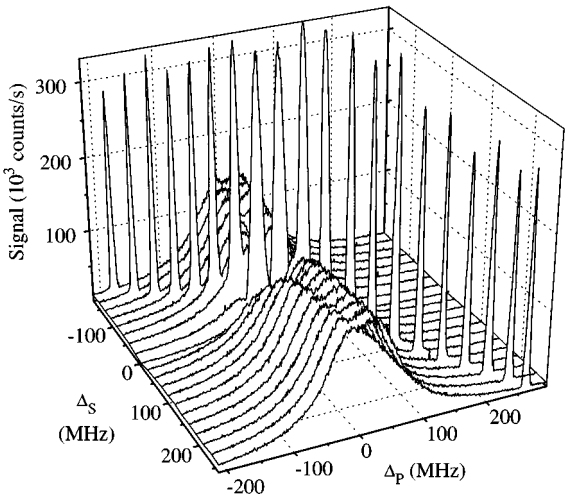

FIG. 9. Population transfer out of the initial state $^3P_0$ into the state $M=0$ state of the final level $^3P_2$. The pump-laser frequency is tuned across the one- and two-photon resonance region while the Stokes-laser frequency is changed in increments of about 23 MHz. The intensities are $I_P=2.7$ mW and $I_S=25$ mW. A small magnetic guiding field had been applied.

may occur by stray light from the pump laser upstream of the STIRAP transfer zone, while stray light from the Stokes laser will be responsible for loss of population of the $^3P_2$ level between the transfer and the detection region.

B. The four- and five-state case

Coupling schemes leading to four- and five-state systems are shown in the uppermost panel of Figs. 10–12. The other panels of those figures display the variation of the eigenvalues and reveal why population transfer is possible or why it fails. Related experimental results are presented in Figs. 13–15.

Figures 10 and 13 refer to pump-laser polarization parallel to the magnetic-field direction ($\beta_P=0°$). The Stokes-laser polarization is perpendicular to **B** ($\beta_S=90°$) and it's frequency is tuned to one-photon resonance for $B=0$. In this case only one state of the intermediate level is involved, while two states of the final level can be reached, depending on which one is in two-photon resonance. Throughout the interaction there exists a dressed state with a zero eigenvalue [see Fig. 10(a)] and efficient transfer is possible for those parameters given. For $B=0$, the states $M=\pm 1$ are degenerate and both receive population.

As the magnetic-field B increases, the degeneracy is removed. Only one of those states may remain in exact two-photon resonance. However, as long as the splitting is small, nonadiabatic coupling will channel some population to the other state. This is illustrated by the two thick lines in panel (b) of Fig. 10 and is demonstrated by the broadening of the peaks in Fig. 13 for small values of B. When the data for this figure, as well as those for Figs. 14 and 15 were taken, the probe-laser intensity was sufficiently high to induce power broadening which exceeds the Zeeman splitting. Therefore there is no M-state selectivity provided by the detection process. The population of all M states is monitored with (nearly) uniform detection efficiency.

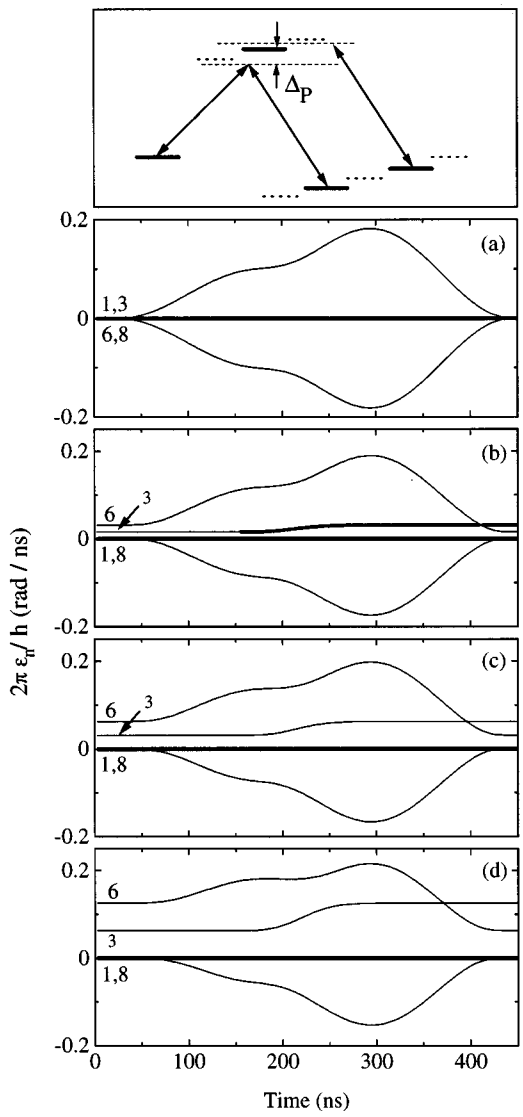

FIG. 10. The uppermost panel shows the states which are coupled for $\beta_P = 0°$ and $\beta_S = 90°$ as heavy lines. The nonparticipating states of the nine-state system are shown as dotted lines. Here only *one state* of the intermediate level is involved. The panels (a)–(d) show the evolution of the eigenvalues as the magnetic field is increased.

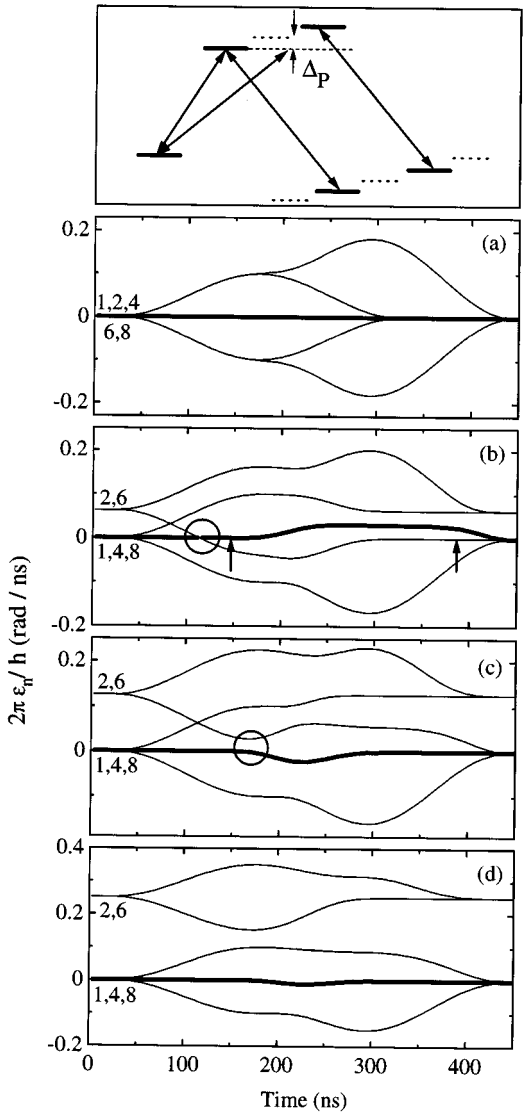

FIG. 11. The uppermost panel shows the states which are coupled for $\beta_P = 90°$ and $\beta_S = 0°$ as heavy lines. The nonparticipating states of the nine-state system are shown as dotted lines. Here *two states* of the intermediate level are involved. The panels (a)–(d) show the evolution of the eigenvalues as the magnetic field is increased.

When the Zeeman splitting exceeds the two-photon resonance width, we essentially recover the ''ideal'' three-state situation 10d. Non-negligible coupling only exists to either $M = +1$ or $M = -1$, depending on the tuning of the laser frequencies. Two separate peaks are seen in Fig. 13 for larger values of B as the pump-laser frequency is tuned. This is an example of the experimental control of the orientation of an angular momentum simply by tuning the frequency of one laser.

For $\beta_P = 90°$ and $\beta_S = 0°$ the states $M = \pm 1$ of the intermediate level are coupled to the initial state by the pump laser and to the state with the same M quantum number in the final level. Figures 11 and 14 show the variation of the eigenvalues and transfer efficiency (as the pump-laser frequency is tuned and the B field is increased in increments) when the Stokes laser is tuned to one-photon resonance. The corresponding set of data for off-resonance tuning of the Stokes laser is shown in Figs. 12 and 15. The fact that there are two states of the intermediate level involved may lead to significant differences in the transfer process as compared to those shown in Figs. 10 and 15. This is particularly true when the Stokes laser frequency is tuned to one-photon resonance, a situation which we discuss next.

Figures 11 and 14 show a striking example of what was identified as ''the connectivity problem'' in papers I and II. The experiment demonstrates, see Fig. 14, that the participation of two (rather than only one) states of the intermediate level is not detrimental to efficient population transfer for very small magnetic fields (lacking M-state selectivity) or for fields exceeding $B = 10$ G, which allow transfer to either $M = +1$ or $M = -1$, depending on laser frequency tuning. Population transfer fails altogether for intermediate strength of the fields, $3 < B < 6$ G. The reason for the breakdown of

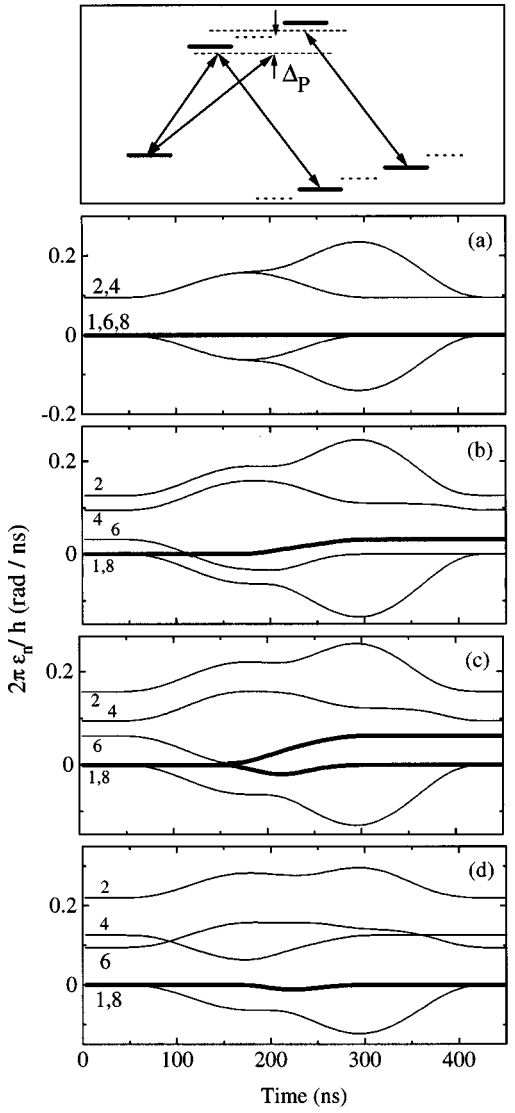

FIG. 12. Same as in Fig. 11, but with the Stokes- and pump-laser frequency *detuned* from one-photon resonance.

the transfer efficiency is revealed in Fig. 11. For $B=0$, there exists a zero eigenvalue state throughout the interaction. The inital state is associated with the zero eigenvalue at early times whereas the final state is related to the zero eigenvalue at late times. For small B, an early (near) crossing of eigenvalues is recognizable. In the present case, the system passes through this crossing region diabatically, because the coupling of the related states depends on the pump-laser intensity, which is still weak. The subsequent adiabatic path, however, does not connect to the state with zero eigenvalue at late times. The system returns to the intial state and population transfer fails. As B increases, the crossing of eigenvalues occurs at a later time, where coupling is stronger and a clearly avoided crossing results, see panel (c) of Fig. 11. The system follows the adiabatic path through this region and smoothly connects to the zero eigenvalue state at late times. Although the deviation of the eigenvalue from zero at intermediate times along this path suggests the risk of some radiative loss of population during the process, a high transfer efficiency is obtained. The influence of avoided crossings is

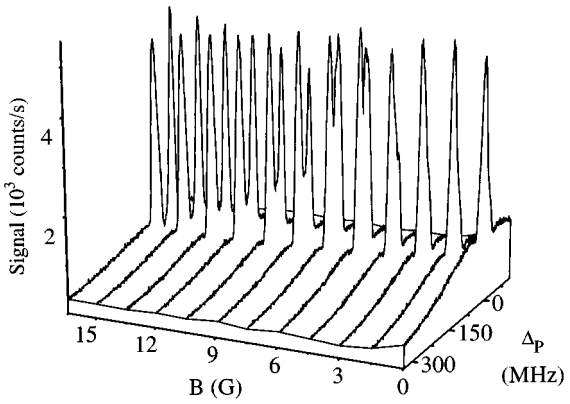

FIG. 13. Population transfer as the magnetic-field strength B is changed. Polarization angles with respect to the magnetic-field direction are $\beta_P=0°$ and $\beta_S=90°$, leading to the coupling of four states with one initial, one intermediate, and two final states. The Stokes-laser frequency is held 200 MHz off the one-photon resonance (which exceeds the Zeeman splitting) while the pump-laser frequency is tuned and the magnetic-field strength is increased in increments. The evolution of the related eigenvalues is shown in Fig. 10. Laser powers are $I_P=$ 56 mW, $I_S=$ 70 mW. For the largest B fields shown selective transfer to $M=+1$ and $M=$-1 is clearly resolved.

hardly discernible at even stronger magnetic fields, see panel (d) of Fig. 11.

Detuning from the one-photon resonance may cure the problem recognized above. Such detuning removes some of the dressed-state degeneracies at early and late times. A state with a zero eigenvalue throughout the interaction is only found for $B=0$. As stated previously this state allows efficient population transfer. For large values of B [panel (d) of

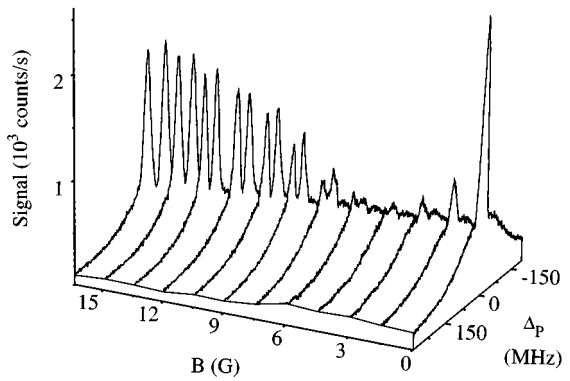

FIG. 14. Population transfer as the magnetic-field strength B is changed. Polarization angles with respect to the magnetic field direction are $\beta_P=90°$ and $\beta_S=0°$. Here the Stokes laser frequency is tuned to (near) resonance with the one-photon transition frequency (see Fig. 11). For small magnetic-field strength $B\approx 0$ the population transfer breaks down but recovers for larger B. This is an example of the lack of an adiabatic transfer path from the initial to the final state. The peaks near $B=15$ G are lower than the one at $B=0$ because the probe-laser frequency is tuned to the $M=0\Leftrightarrow M'=0$ resonance and thus excites the transitions starting at $M=\pm 1$ only in the wings of their profile. The actual transfer efficiency also approaches 100% in this case. The evolution of the related eigenvalues is shown in Fig. 11.

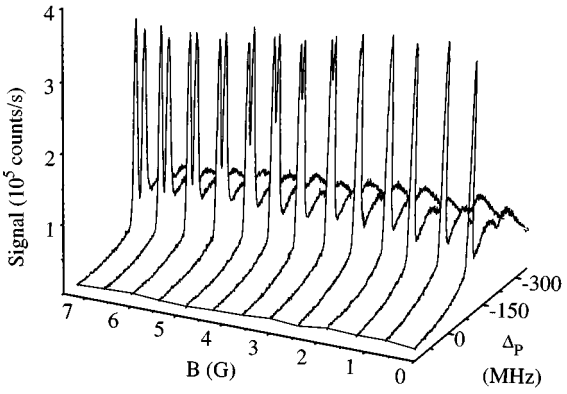

FIG. 15. Population transfer as the magnetic field-strength B is changed. Polarization angles with respect to the magnetic-field direction are $\beta_P = 90°$ and $\beta_S = 0°$, leading to the coupling of five (out of nine) states with one initial, two intermediate, and two final states. The Stokes-laser frequency is held 200 MHz off the one-photon resonance (which exceeds the Zeeman splitting) while the pump-laser frequency is tuned and the magnetic-field strength is increased in increments. Laser powers are $I_P = 28$ mW, $I_S = 47$ mW. For the largest B fields shown selective transfer to $M = +1$ and $M = -1$ is clearly resolved. The evolution of the related eigenvalues is shown in Fig. 12.

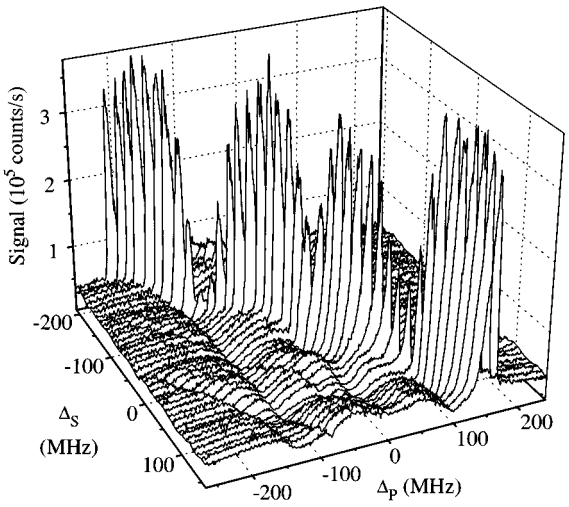

FIG. 16. Population transfer to the $M = 0$ final state for polarization angles $\beta_P = 20°$ and $\beta_S = 60°$, with respect to the magnetic-field direction. In this case, all nine states are radiatively coupled. The magnetic-field strength is $B = 70$ G. The pump-laser frequency is tuned across the resonance region while the Stokes-laser frequency is changed in increments. Efficient population transfer is achieved for two-photon resonance ($\Delta_P = \Delta_S$) but three regions of reduced transfer efficiency are identified. The origin of the breakdown of the transfer efficiency and the structure of the signal away from the two-photon resonance is explained in the text. Laser powers are 65 mW for the pump and 60 mW for the Stokes laser.

Fig. 12] we also identify an eigenstate with a (nearly) zero-energy eigenvalue and all the other eigenvalues well separated from it. This is the scenario for successful completion of efficient and selective population transfer. At intermediate values of B the splitting of eigenvalues may be small enough to allow population transfer to more than one single M state by nonadiabatic coupling. However, a ''connectivity problem'' does not develop. Considering the sum of the population reaching these M states, we expect high transfer and demonstrate it (Fig. 15).

C. The nine-state case

When none of the laser polarizations is parallel or perpendicular to the magnetic field there are no simplifying symmetries. All states are involved in the coupling scheme and we need to consider a nine-state system. The relative strength of the various coupling paths can be controlled, within the limits imposed by the geometric line strength factors, by choosing a particular set of polarization angles β_S and β_P.

Figures 16–19 show, for specific sets of parameters β and magnetic-field strength, population transfer to individual M states of the final level. These figures reveal characteristic properties of the transfer process. The pump-laser frequency varies continuously for a set of discrete frequencies of the Stokes laser. The Rabi frequencies are large enough to satisfy the adiabaticity criterion when conditions for efficient transfer are met. The Zeeman splitting is also sufficiently large, and the probe-laser intensity is sufficiently small, that power broadening does not prevent selective detection of the population of individual M states. The following pictures will therefore show ''STIRAP ridges'' determined by the respective two-photon resonance line ($\Delta_S = \Delta_P$). Along those ridges we find locations where the transfer efficiency is reduced or where transfer is not possible.

The STIRAP ridges stand on a structured background, which is mainly caused by spontaneous emission into the particular M state monitored by the probe laser. This structure is sufficiently interesting to warrant brief comment. When the pump laser is tuned to resonance with one of the intermediate states which is radiatively connected to the probed M state, but two-photon resonance is not established, then a saturation broadened ''spontaneous emission ridge'' is observed. This enhanced population is independent of the Stokes-laser tuning and thus runs parallel to the Δ_S scale. A clear example of such a structure is seen in Fig. 17 for $\Delta_P = 0$. On the other hand, when the pump-laser frequency is tuned into resonance with an intermediate state that has a relatively large radiative transition rate to an M state other than the monitored one, population by spontaneous emission will preferentially reach those states and a ''spontaneous emission valley'' develops. Examples of such a structure are seen in Figs. 16 and 19 (upper panel) near $\Delta_P = 100$ MHz, running again parallel to the Δ_S scale.

The spontaneous background is different for $\beta_P = 20°$ and $\beta_P = 60°$. The $M = 0$ state in the intermediate level receives significantly more population in the first case. Decay to the $M = 0$ state of the final level generates a broad spontaneous emission ridge. Narrow valleys develop near the $M = \pm 1$ one-photon resonances, because coupling to the $M = \pm 1$ intermediate states is weak and decay is predominantly to states other than the target $M = 0$ state.

Finally, when the two-photon resonance condition is met for a state other than the monitored one, we observe a structure which runs parallel to the main STIRAP ridge. This structure may be a valley, as in Fig. 16, or a small satellite

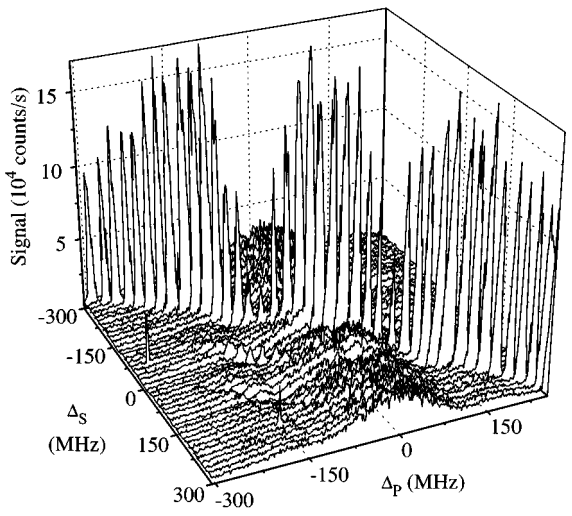

FIG. 17. Population transfer to the $M=0$ final state for polarization angles $\beta_P=\beta_S=60°$, with respect to the magnetic-field direction. The Zeeman splitting is about 140 MHz. The breakdown of the transfer efficiency, despite the two-photon resonance ($\Delta_P=\Delta_S$) occurs because of the lack of an adiabatic transfer path connecting the initial and final state.

ridge, as in Fig. 19. A valley develops when efficient coherent population transfer occurs to one of the neighboring states which is not monitored by the probe laser. This leads to a dark resonance in the spontaneous emission channels, see Fig. 16. A small satellite ridge develops when the saturation broadening of the probe-laser transition is a bit too large (compared to the Zeeman splitting) for single M-state detection and thus the detection efficiency for this neighboring state is not exactly zero. The loss of spontaneous emission to a particular M state may therefore be overcompensated by the small detection probability for the population which reaches another M state. The upper panel of Fig. 19 shows a STIRAP ridge for transfer to $M=-1$ in the final level. We also recognize a satellite ridge when transfer occurs to $M=0$. The detection probability for the state $M=+1$ is negligibly small. There is a valley related to the dark resonance when coherent population transfer to this state occurs.

Figure 16 shows two pronounced notches in the STIRAP ridges. These notches demonstrate failure of coherent population transfer because the adiabatic states leading from the initial to the final state do not connect. The signal along this ridge seen in Fig. 17 is reproduced in Fig. 18. The regions of expected failure of efficient population transfer, according to Eq. (4.14) of Ref. [22] is marked. There is very good agree-

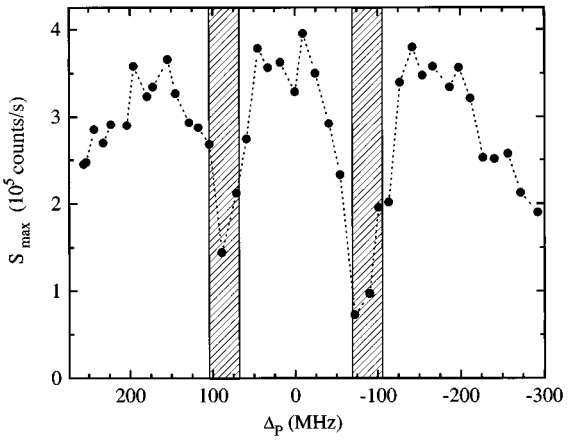

FIG. 18. Maxima of the transfer signal for two-photon resonance as a function of pump-laser detuning, taken along the ''STIRAP ridge'' shown in Fig. 17. The vertical lines mark the pump-laser detuning range 70 MHz$<|\Delta_P|<$105 MHz for which the breakdown of the transfer efficiency is expected, according to Eq. (4.14) of Ref. [22], in excellent agreement with the experiment.

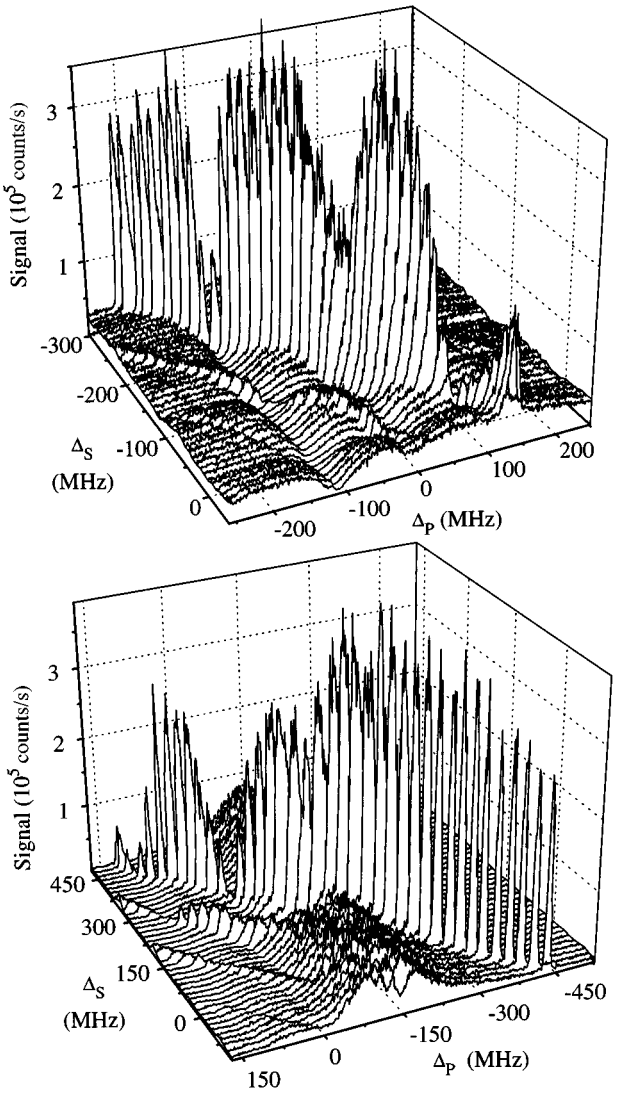

FIG. 19. Population transfer to the $M=-1$ final state for polarization angles $\beta_P=20°$ and $\beta_S=60°$, with respect to the magnetic-field direction (a) and transfer to the $M=2$ state with $\beta_P=\beta_S=60°$ (b). Along the STIRAP ridge there are regions where population transfer fails. The small ridges that run parallel to the main two-photon resonance ridge are seen because the saturation broadening of the probe laser is sufficiently large to also excite the states $M=\pm1$ and $M=\pm2$ with very small excitation probability, when the two-photon resonance conditions, leading to population transfer, is established for these states.

ment of the result from this equation and the experimental observation.

Figure 19 shows the transfer to $M=-1$ (upper level) and $M=2$ (lower panel), for the same polarizations as in Fig. 16. The notches in the STIRAP ridge are either due to spontaneous emission losses or caused by the connectivity problems. The agreement between the measured data and the numerical results shown in Figs. 16(b) and 16(c) of Ref. [21] is very good.

D. Dependence of transfer on Rabi frequency

As shown above, the polarization angles and laser frequency detunings affect success or failure of population transfer in a multistate system. Other important parameters are the several Rabi frequencies. It is well established for a three-state system that population transfer is complete when the Rabi frequencies are sufficiently large to satisfy the adiabaticity condition. The robustness of the transfer process increases with increasing Rabi frequencies. However it is important to recognize that this advantage of increased laser power does not always apply for multistate systems. In these more general systems, the Rabi frequencies are but additional parameters which control adiabatic energy splittings. The changes of adiabatic energy curves may introduce or alter curve crossings. As we have shown in papers I and II, and in the present work, level crossings may either be detrimental or beneficial for population transfer.

In Fig. 20 we demonstrate this observation with examples of population transfer for two different coupling schemes. In the upper frame the polarization angles are such that we have only one intermediate state; in the lower frame the polarization angles permit two intermediate states. In the upper frame, with only one intermediate state, population transfer is complete when pump-laser power exceeds 15 mW. Further increase of pump-laser power broadens the two-photon linewidth but is not detrimental to the population transfer. In the lower frame, population transfer is efficient for low pump-laser power of 3 mW, but fails for higher power.

Inspection of the dressed-state eigenvalue curves provides the explanation for this different behavior. When two intermediate states are involved, curve crossings may block the adiabatic path which connects the initial and final state. As we have mentioned earlier when discussing effects of other parameters, such connectivity problems are avoided if the laser frequencies are tuned sufficiently far from any one-photon resonance with one of the intermediate states. The essential conclusion to be drawn from such observations is that for efficient population transfer the two-photon linewidth should not exceed the intermediate level separation, if the laser frequencies are close to one-photon resonance.

IV. SUMMARY AND CONCLUSION

We have presented experimental confirmation of all the features of STIRAP predicted in papers I and II. Specifically, we have shown examples of experimental conditions that lead to successful population transfer into a selected final magnetic sublevel, and we have shown examples in which population transfer does not occur. The latter examples, discussed in detail, show that caution is needed when STIRAP is applied to multistate systems.

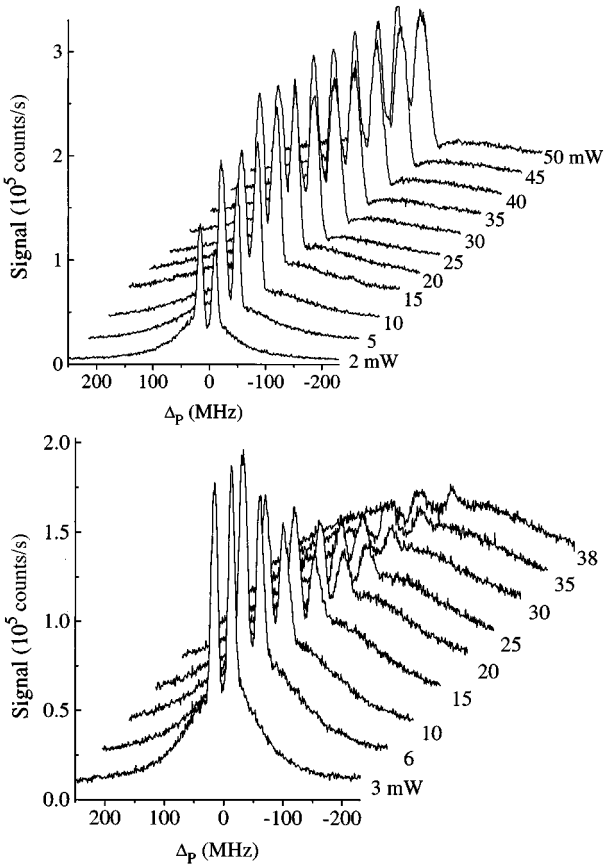

FIG. 20. Examples of the variation of the efficiency of population transfer with increasing Rabi frequency. In both cases we have two final states. In case (a) the coupling scheme is such that we have only *one* intermediate state ($\beta_P=0°, \beta_S=90°$). The transfer efficiency increases with increasing Rabi frequency. Panel (b) shows an example of decreasing efficiency of population transfer with increasing Rabi frequency. The coupling scheme is such that we have *two* intermediate states ($\beta_P=90°, \beta_S=0°$). The magnetic-field strength is 7.5 G. Both pump and Stokes laser have the same power as indicated in the figure.

An important conclusion, predicted theoretically and now confirmed in experiment, concerns the undesirability of maintaining one-photon resonance conditions (in addition to the required two-photon resonance) when more than three levels are involved. Although the coupling is strongest for one-photon resonance, this condition may lead to transient population accumulation in intermediate states. Such population is subject to spontaneous emission, and hence this situation will not have optimum population transfer into the final state.

Detrimental effects may also occur when either the pump or Stokes laser is tuned between energies of Zeeman-split sublevels. In one of our examples the detuning was midway ($\beta_P=\beta_S=60°$) and in another example close to an one-photon resonance ($\beta_P=20°$, $\beta_S=60°$). At such detunings the interaction between dressed-state eigenvalues may, depending on Rabi frequencies, prevent connection of the initial and final adiabatic states.

Furthermore, we have experimentally analyzed a model system with multiple coupling paths between initial as well as final and closely spaced intermediate states. If the detun-

ings are close to one-photon resonance and the width of the two-photon resonance exceeds the intermediate state separation, population transfer fails. When care is taken to avoid such detrimental effects, it is possible to achieve complete population transfer in systems that have magnetic sublevels.

ACKNOWLEDGMENTS

We thank H. Hotop for kindly providing the initial version of the beam source. We also thank H.-G. Rubahn, E. Konz, and T. Kraft for assistance during preliminary work towards this experiment. We acknowledge support from the Deutsche Forschungsgemeinschaft, the EU network ''Laser Controlled Dynamics of Molecular Processes and Applications,'' ERB-4050PL93-2602., a NATO collaborative research grant and from the Stiftung für Innovation Rheinland-Pfalz through the laser center at Kaiserslautern. The work of B.W.S. is supported in part under the auspices of the U.S. Department of Energy at Lawrence Livermore National Laboratory under Contract No. W-7405-Eng-48.

[1] J. Oreg, F.T. Hioe, and J.H. Eberly, Phys. Rev. A **29**, 690 (1984).
[2] U. Gaubatz, P. Rudecki, M. Becker, S. Schiemann, M. Külz, and K. Bergmann, Chem. Phys. Lett. **149**, 463 (1988).
[3] U. Gaubatz, P. Rudecki, S. Schiemann, and K. Bergmann, J. Chem. Phys. **92**, 5363 (1990).
[4] J.R. Kuklinski, U. Gaubatz, F.T. Hioe, and K. Bergmann, Phys. Rev. A **40**, 6741 (1989).
[5] C. Liedenbaum, S. Stolte, and J. Reuss, Phys. Rep. **178**, 1 (1989).
[6] J. Reuss and N. Dam, in *Applied Laser Spectroscopy*, edited by M. Inguscio and W. Demtröder (Plenum, New York, 1990).
[7] N. Dam, L. Oudejans, and J. Reuss, Chem. Phys. **140**, 217 (1990).
[8] B. Broers, H.B. van Linden van den Heuvell, and L.D. Noordam, Phys. Rev. Lett. **69**, 2062 (1992).
[9] P. Marte, P. Zoller, and J.L. Hall, Phys. Rev. A **44**, 4118 (1991).
[10] L.S. Goldner, C. Gerz, R.J. Spreeuw, S.L. Rolston, C.I. Westbrook, W.D. Phillips, P. Marte, and P. Zoller, Phys. Rev. Lett. **72**, 997 (1994).
[11] J. Lawall and M. Prentiss, Phys. Rev. Lett. **72**, 993 (1994).
[12] M. Weitz, B.C. Young, and S. Chu, Phys. Rev. Lett. **73**(19), 2563 (1994).
[13] K. Bergmann and B.W. Shore, in *Molecular Dynamics and Spectroscopy by Stimulated Emission Pumping*, edited by H.L. Dai and R.W. Field (World Scientific, Singapore, 1995).
[14] C.E. Carroll and F.T. Hioe, Phys. Rev. Lett. **68**, 3523 (1992).
[15] A.S. Parkins, P. Marte, P. Zoller, and H.J. Kimble, Phys. Rev. Lett. **71**, 3095 (1993).
[16] T. Nakajima and P. Lambropoulos, Opt. Commun. **118**, 40 (1995).
[17] G. Coulston and K. Bergmann, J. Chem. Phys. **96**, 3467 (1992).
[18] A. Kuhn, G. Coulston, G.Z. He, S. Schiemann, K. Bergmann, and W.S. Warren, J. Chem. Phys. **96**, 4215 (1992) .
[19] S. Schiemann, A. Kuhn, S. Steuerwald, and K. Bergmann, Phys. Rev. Lett. **71**, 3637 (1993).
[20] B.W. Shore, K. Bergmann, and J. Oreg, Z. Phys. D **23**, 33 (1992).
[21] B.W. Shore, J. Martin, M.P. Fewell, and K. Bergmann, Phys. Rev. A **52**(1), 566 (1995).
[22] J. Martin, B.W. Shore, and K. Bergmann, Phys. Rev. A **52**, 583 (1995).
[23] B.W. Shore, *The Theory of Coherent Atomic Excitation* (Wiley, New York, 1990).
[24] B.W. Shore, K. Bergmann, J. Oreg, and S. Rosenwaks, Phys. Rev. A **44**, 7442 (1991).
[25] A.V. Smith, J. Opt. Soc. Am. B **9**, 1543 (1992).
[26] M.J. Verheijen and H.C.W. Beijerinck, Chem. Phys. **102**, 255 (1986).
[27] H. Hotop, in *Methods of Experimental Physics*, edited by F.B. Dunning and R. Hulet (Academic, New York, 1996), Vol. II.
[28] J.P.C. Kroon, H.C.W. Beijerinck, and B.J. Verhaar, Chem. Phys. **90**, 195 (1984).